Dynamics and Efficiency of Electron Injection and Transport in DNA Using Pyrenecarboxamide as an Electron Donor and 5-Bromouracil as an Electron Acceptor†

Pierre Daublain,‡ Arun K. Thazhathveetil,‡ Vladimir Shafirovich,*,§ Qiang Wang,|| Anton Trifonov,|| Torsten Fiebig,*,|| and Frederick D. Lewis*,‡

Department of Chemistry, Northwestern University, Evanston, Illinois 60208-3113, Department of Chemistry, Boston College, Chestnut Hill, Massachusetts 02467, and Department of Chemistry, New York University, New York, New York 10003

Received: November 11, 2009; Revised Manuscript Received: January 12, 2010

The photophysical and photochemical behavior of a series of hairpin-forming DNA conjugates possessing a 5′-tethered pyrenecarboxamide chromophore and one or two bromouracil bases has been investigated. Quenching of the pyrene fluorescence and transient absorption spectra characteristic of the pyrene cation radical are observed only when bromouracil is located at the first or second base pair position nearest to the point of pyrene attachment. These observations are consistent with an intercalated structure for these conjugates in which pyrene is adjacent to the second base pair. Selective quenching of singlet pyrene by bromouracil but not by thymine is consistent with the free energy for charge separation estimated using Weller's equation. Low quantum yields for loss of bromide when bromouracil is not adjacent to pyrene are attributed to inefficient charge separation via either a multistep electron transport or a single-step superexchange mechanism. Quantum yields are only weakly dependent upon the distance between pyrene and bromouracil, as expected for a multistep electron transport mechanism. Loss of bromide from conjugates possessing two bromouracils occurs sequentially. For adjacent bromouracils, competitive loss of bromide from both bromouracils is observed, whereas for nonadjacent bromouracils loss of bromide from the proximal bromouracil occurs prior to any loss from the distal bromouracil, consistent with a slower rate constant for electron transport vs loss of bromide.

Introduction

Charge separation over multiple base pairs in DNA can occur via either the migration of positive charge (holes) or negative charge (electrons).[1] Experimental studies of the dynamics and efficiency of photoinduced hole transport have been more numerous than measurements of electron transport. Reasons for this include the lower potentials for oxidation of the purines A and G vs reduction of the pyrimidines T, C, and U (Chart 1a)[2] and the ability of G to serve as a hole trap capable of undergoing hole transport between G-containing sites in competition with oxidative strand cleavage. The pyrimidines have similar reduction potentials, and thus none can serve as an electron trap. Thymine dimer,[3−6] thymine oxetane,[7] and the halouracils[8−10] have been employed as electron traps in investigations of electron transport in DNA. The thymine dimer and thymine oxetane undergo cycloreversion, and the halouracils undergo loss of halide ions upon reduction. Most investigations of distance-dependent DNA electron transport have employed irreversible methods of electron injection, including photoinduced charge shift from a reduced flavin,[6,7] ground state electron transfer from a ketyl radical anion[5] or a reduced irridium(II) complex,[10] or pulse radiolysis.[11] These studies have established that the characteristic reactions of electron traps are only weakly dependent upon the number or sequence of base pairs separating the trap from the point of injection. However, the use of irreversible methods precludes investigation of the dynamics of electron injection.

We recently reported the results of an investigation of the dynamics of photoinduced electron injection and the distance dependence of the efficiency of electron transport in DNA using a 5′-tethered aminopyrene (APy, Chart 1b) hairpin possessing bromo- and iodouracil (^{X}U) as electron acceptors separated from APy by one or more A−T base pairs (Chart 1c).[12] APy is a strong electron donor capable of reducing adjacent T or ^{X}U bases with subpicosecond (ps) time constants for electron injection (Figure 1a). Charge recombination in the resulting radical ion pair is more rapid than electron transport and loss of halide ions, leading to low quantum yields for dehalogenation. These observations are consistent with previously reported studies of photoinduced charge separation using ^{X}U bases as electron acceptors in which neither long-lived charge-separated states nor efficient loss of halide ions were observed.[13] It occurred to us that the use of a less potent electron donor might effect selective reduction of ^{X}U and thus permit investigation of electron injection via a single-step superexchange process. Use of a weaker electron donor might also slow down charge recombination, thus permitting electron transport to compete more effectively with charge recombination.

We report here the results of a collaborative investigation of the dynamics of electron injection and the efficiency of ^{Br}U dehalogenation in a family of hairpins (Chart 1c) possessing a 5′-pyrenecarboxamide electron donor (PyA, Chart 1b) and either one or two ^{Br}U−A base pairs separated by a variable number of A−T base pairs. We have previously observed that singlet PyA can serve as a hole donor for the selective oxidation of G vs A (Figure 1b).[14] We now find that PyA can serve as a selective electron donor for the reduction of ^{Br}U vs T. The

† Part of the "Michael R. Wasielewski Festschrift".

* Corresponding authors. E-mail: fdl@northwestern.edu; vs5@nyu.edu; fiebig@bc.edu.

‡ Northwestern University.

§ New York University.

|| Boston University.

10.1021/jp9107393
Published on Web 02/02/2010

CHART 1: (a) Purines Adenine (A) and Guanine (G) and Pyrimidines Thymine (T), 5-Bromouracil (^{Br}U), and Uracil (U) and Their Redox Potentials, (b) Pyrene Derivatives Aminopyrene (APy), Pyrenecarboxamide (PyA), Their Singlet Energies, and Redox Potentials, (c) Pyrene Conjugates and Control Hairpins, and (d) the Dyad PyA-PI

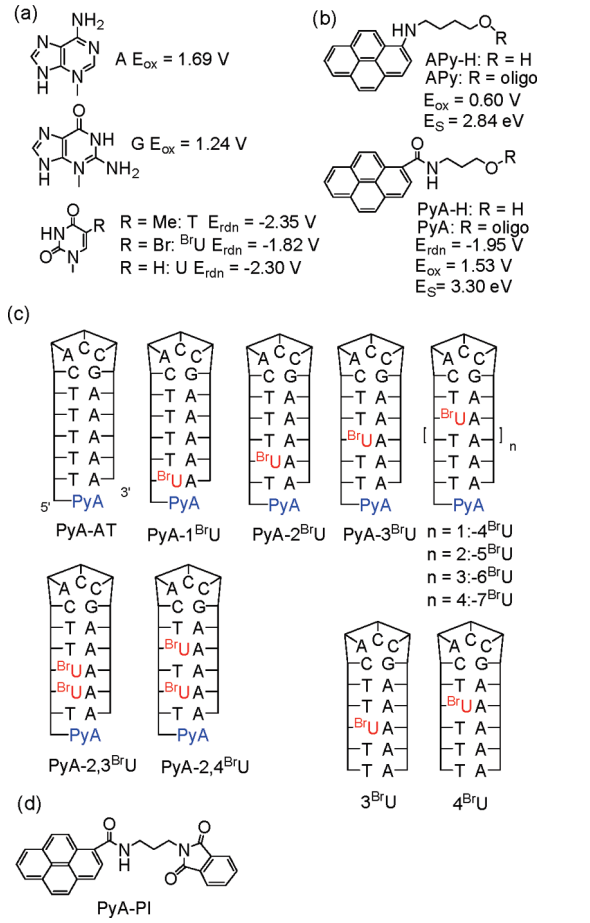

dynamics of both charge separation and charge recombination with neighboring ^{Br}U are slower for PyA vs APy, in accord with the higher oxidation potential for PyA (Chart 1b). However, the efficiency of superexchange electron transfer is too low to be detected with either PyA or APy. The distance dependence and absolute values of the quantum yields for loss of halide ion from ^{Br}U are similar for the two pyrene derivatives. Conjugates possessing two adjacent ^{Br}U bases undergo competitive loss of halide ions, whereas conjugates possessing two ^{Br}U bases separated by a single T undergo loss of bromine from the ^{Br}U proximate to the PyA prior to loss of bromine from the distal ^{Br}U, consistent with the function of ^{Br}U as a deep electron trap on the time scale of electron transport.

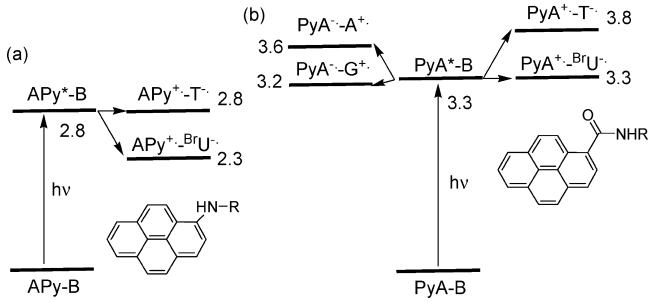

Figure 1. Energetics of charge separation for (a) aminopyrene (APy) and (b) pyrenecarboxamide (PyA) with selected nucleobases (B). Energies are in electronvolts.

Experimental Section

General Procedures. UV absorption, fluorescence, and circular dichroism spectra were obtained as previously described on samples contained in 1 cm path length cuvettes.[12,15] Quantum yields for fluorescence were determined using quinine sulfate in sulfuric acid as a reference standard.[16] CD spectra are the average of two scans with a data interval of 1.0 nm and a time interval of 2 s per point. The base lines are corrected by subtraction of the spectrum of the buffer (10 mM phosphate, 0.1 M NaCl). Electrochemical measurements were performed using a CH Instruments model 622 electrochemical workstation. The solvent was dimethyl formamide containing a 0.1 M tetra-*n*-butylammonium hexafluorophosphate electrolyte. A glassy carbon working electrode, platinum wire counter electrode, and Ag/AgCl reference electrode were employed. Ferrocene/ferrocinium (Fc/Fc^{+}, 0.47 vs SCE in DMF[17]) was used as an internal reference for all measurements.

All samples for kinetic spectroscopic measurements were prepared in 10 mM sodium phosphate, pH 7.2, buffer with 0.1 M NaCl (standard buffer). Samples were stirred during these measurements and absorption spectra checked before and after spectroscopic studies for the occurrence of decomposition. Hairpin concentrations were adjusted to provide an absorbance of 0.2 at 354 nm in a 1 cm path length cuvette for fluorescence measurements and 0.27 in a 1 mm path length cell for pump−probe measurements. Fluorescence decay measurements, nanosecond transient absorption measurements, and femtosecond broadband pump−probe spectra were obtained as previously described.[12,15]

Samples of hairpin conjugates for quantitative photochemical studies having an optical density of 0.02 at 355 nm were prepared in standard buffer containing 0.1 M isopropyl alcohol (*i*-PrOH). Samples (1.7 mL) were placed in quartz cuvettes equipped with a stirring bar and a rubber septum and were purged with dry nitrogen for 15 min prior to irradiation. Samples were irradiated in a thermostatted cuvette holder at 20 °C with monochromatic 355 nm light provided by a 150 W mercury arc lamp and a 0.5 M monochromator. For HPLC analysis, 5.0 μL aliquots were withdrawn by syringe at regular time intervals and analyzed by HPLC using a Varian Microsorb-MV100 C18 column on a Dionex HPLC system equipped with a diode array detector. Solutions of (A) 0.03 M TEAA and (B) 95% acetonitrile and 5% 0.03 M TEAA were used as the mobile phase. A gradient of 5 min 0−16% B, followed by an isocratic elution (16% B−84% A) with a flow rate of 1 mL/min was used for the separation. Integration of HPLC peaks using detection wavelengths of 260 nm (base pair) and 355 nm (pyrene) provided similar results. For MALDI analysis, the overlapping reactant and product peaks were collected by HPLC, and the solvent was evaporated and the residue dissolved in 10 μL of water. Half of this solution was used to prepare five spots on the MALDI plate. Integrated HPLC or MALDI peak areas were used to construct plots of % conversion vs irradiation time. Relative quantum yields were determined from the initial slopes of these plots. Absolute quantum yields for **APy-4^{Br}U** were determined at low conversions (<25%) of reactant to product (average of three independent HPLC analyses) using potassium ferrioxalate actinometry to determine the intensity of absorbed light.[18] The resulting quantum yield was used to convert the relative quantum yields to absolute quantum yields.

Materials

***N*-((3-Dioxoisoindolin-2yl)propyl)pyrene-1-carboxamide (PyA-PI).** *N*-(3-Aminopropyl)phthalimide was prepared from the reaction of phthalimide with Boc-protected 3-chloro-1-aminopropane by the method of Alfred et al.[19] Reaction of the acid chloride of pyrene-1-carboxylic acid with the deprotected *N*-(3-aminopropyl)phthalimide afforded **PyA-PI**. Mp 172−174 °C. ^{1}H NMR (500 MHz; $CDCl_3$): δ (ppm) 8.6 (1H, d, $J = 9.2$ Hz), 8.0−8.2 (8H, m, Py−H), 7.73 (2H, dd, $J1 = 3.1$, $J2 = 5.2$ Hz, An−H), 6.95 (1H, bt, N−H), 3.9 (2H, t), 3.8 (2H, m), 3.6 (2H, $J = 6.1$, m), 2.09 (2H, $J = 6.1$, q). ^{13}C NMR δ (ppm) 170.0, 168.7, 133.9, 132.4, 131.7, 131.1, 130.9, 130.6, 128.6, 128.5, 127.0, 126.2, 125.7, 125.6, 124.7, 124.5, 124.4, 124.3, 123.2, 36.9, 35.2, 28.5.

PyA-H was prepared and converted to its phosphoramidite derivative as previously described[14] and attached to the 5′-terminus of an oligonucleotide using conventional solid supported oligonucleotide synthesis. The conjugates were deprotected using 30% ammonium hydroxide and purified by RP HPLC. Structures were confirmed by MALDI-TOF-MS (Table S1, Supporting Information), and the purities were confirmed by analytical HPLC.

Results

Electronic Spectra of the Pyrene Derivatives. The preparation and characterization of **PyA-H** and **PyA-AT** have previously been described.[14] Preparation of the dyad **Py-PI** and the ^{Br}U-containing PyA conjugates is described in the Experimental Section. Conjugates **PyA-AT** and **PyA-3^{Br}U** have melting temperatures $T_m = 60.0$ and 63.0 °C, respectively (Figure S1, Supporting Information), determined from the derivatives of 260 nm thermal dissociation profiles. The circular dichroism spectra of the **PyA** conjugates (Figure S2, Supporting Information) display very weak bands at wavelengths longer than 300 nm attributed to induced CD of the pyrene chromophore and stronger bands between 200 and 300 nm similar to those for the duplex poly(dA):poly(dT).[20]

The absorption and fluorescence spectra of **PyA-H** and **PyA-AT** have been reported.[14] The presence of the amide substituent has little effect on the appearance of the spectra of **PyA-H**, which display vibronic structure similar to that of unsubstituted pyrene.[16] The weak absorption maximum of **PyA-H** at 380 nm is assigned to the pyrene band 1 and the stronger maximum at 341 nm to pyrene band 2. The results of semiempirical ZINDO calculations[21] for *N*-methylpyrene-carboxamide (Figure S3, Supporting Information) are consistent with the assignment of both long-wavelength bands to pyrene-localized $\pi-\pi^*$ transitions. The long-wavelength region ($\lambda > 300$ nm) of the UV spectra of the dyad **PyA-PI** (Chart 1) is superimposable upon that of **PyA-H**, indicative of the absence of ground state electronic interaction between the pyrene and phthalimide chromophore in methanol. The long-wavelength portion of the UV absorption spectra and the fluorescence spectra of the PyA conjugates in aqueous buffer are broadened and red-shifted by several nanometers, when compared to the spectra of **PyA-H** in methanol.

Fluorescence quantum yields and decay times for **PyA-H** and the dyad **PyA-PI** in methanol are reported in Table 1 along with fluorescence data for the PyA conjugates in aqueous buffer (values of Φ_{fl} for conjugates **PyA-*n*^{Br}U** ($n = 5-7$) are the same as those for **PyA-AT** and **PyA-4^{Br}U**, as reported in footnote b). The dyad **PyA-PI** is weakly fluorescent, indicative of efficient intramolecular quenching of PyA fluorescence by the PI electron acceptor. Fluorescence decay times for the PyA conjugates determined with a Ti-Sp-based laser system having a time resolution of ca. 35 ps are best fit as dual exponentials (Table 1). The nanosecond decay components observed for all of the conjugates are assigned to PyA singlet radiative and nonradiative decay. The 140 ps decay component observed for **PyA-1^{Br}U** (140 ps) is tentatively assigned to charge separation.

TABLE 1: Fluorescence Quantum Yields and Decay Times and Transient Kinetics and Assignments for PyA Derivatives and Conjugates

pyrene[a]	Φ_{fl}[b]	τ_s, ns[b,c]	τ (global), ps[d]	470/520 nm, ps[e]
PyA-H	0.30	37		
PyA-PI	0.013		480, L	
PyA-AT	0.38	3.9 (27), 10.7 (73)	6(r), L	
PyA-1^{Br}U	0.031	0.14 (92), 8.0 (8)	10(r), 30(r), 130, L	44(r), 170
PyA-2^{Br}U	0.17	2.1 (24), 10.3 (76)	7(r), 240, L	18(r), 330
PyA-3^{Br}U	0.37	3.7 (29), 10.7 (71)	9(r), L	
PyA-4^{Br}U	0.38	3.8 (26), 10.7 (73)	5(r), L	

[a] See Chart 1 for structures. Values of Φ_{fl} and τ_s for **PyA-H** and **PyA-PI** determined in methanol and values for the PyA conjugates in aqueous buffer. [b] Values of Φ_{fl} and τ_s for conjugates determined in aqueous buffer. Values of Φ_{fl} for **PyA-5^{Br}U**, **-6^{Br}U**, and **-7^{Br}U** are 0.38 ± 0.02. [c] Lifetimes obtained from fluorescence decays with pre-exponentials in parentheses. The long-lived decay for **PyA-1^{Br}U** is the weighted average of two low-amplitude 4.5 (5.2) and 15 (2.6) ns components. [d] Rise (r) and decay times obtained from global fits of the long-wavelength transient absorption bands except for **PyA-1^{Br}U** (fit from rise of 470 nm absorption band) attributed to ^{1}S* relaxation. 30 ps rising component obtained from global fits for **PyA-1^{Br}U** attributed to formation of $PyA^{+\bullet Br}U^{-\bullet}$. Shorter decay times for **PyA-1^{Br}U** and **-2^{Br}U** attributed to formation of $PyA^{+\bullet Br}U^{-\bullet}$. Longer decay times (L > 2 ns) attributed to ^{1}S* decay. [e] Rising (r) and decaying components of band intensity ratio attributed to charge separation (formation of $PyA^{+\bullet Br}U^{-\bullet}$) and charge recombination, respectively.

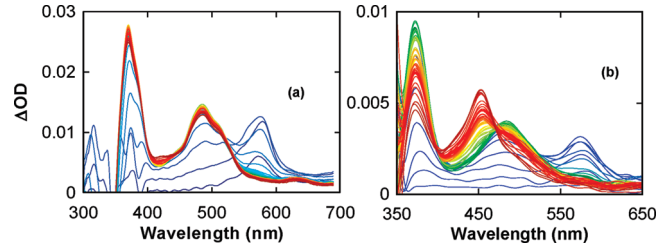

Figure 2. Transient absorption spectra for (a) **PyA-H** (0−10 ps) from ref 14 and (b) **PyA-PI** (0.20−1.8 ns) in methanol. Blue spectra are for early delay times and red spectra for longer delay times. Color code: blue, 0−1 ps; yellow-green, 1−5 ps; and red, >5 ps.

Pump−Probe Spectra of Reference Molecules. Transient spectra for **PyA-H** and **PyA-PI** in methanol obtained using a pump wavelength of 346 nm are shown in Figure 2. As previously reported, the spectra of **PyA-H** display a negative band at 345 nm assigned to the ground state bleach and a positive band at ca. 575 nm assigned to pyrene ^{2}S*, both of which are formed during the pump pulse (Figure 2a).[14] The 575 nm band decays within the first picosecond and is replaced by two bands at shorter wavelengths (370 and 485 nm) assigned to pyrene ^{1}S*. These bands do not decay appreciably during the 1.9 ns time window of our measurements. The appearance of the transient spectra assigned to ^{2}S* and ^{1}S* is similar to that reported for pyrene and several of its derivatives, as is the occurrence of ultrafast internal conversion.[22,23] The long transient decay time for **PyA-H** is consistent with its large fluorescence quantum yield and long fluorescence decay time (Table 1).

The transient spectra for the dyad **PyA-PI** (Figure 2b) display a fast rise and decay of the 575 nm ^{2}S* band, similar to that for **PyA-H** (Figure 2a). This is followed by the growth of a band at 450 nm and a weak shoulder at 420 nm attributed to formation of

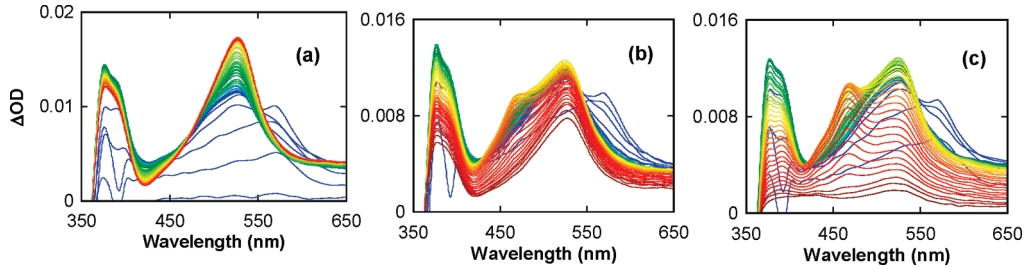

Figure 3. Transient absorption spectra of conjugates (a) **PyA-AT** (data from ref 14), (b) **PyA-1^{Br}U**, and (c) **PyA-2^{Br}U** in aqueous buffer (0.2−1.9 ns). Blue spectra are for early delay times and red spectra for longer delay times. Color code: blue, 0−1 ps; yellow-green, 1−5 ps; and red, >5 ps.

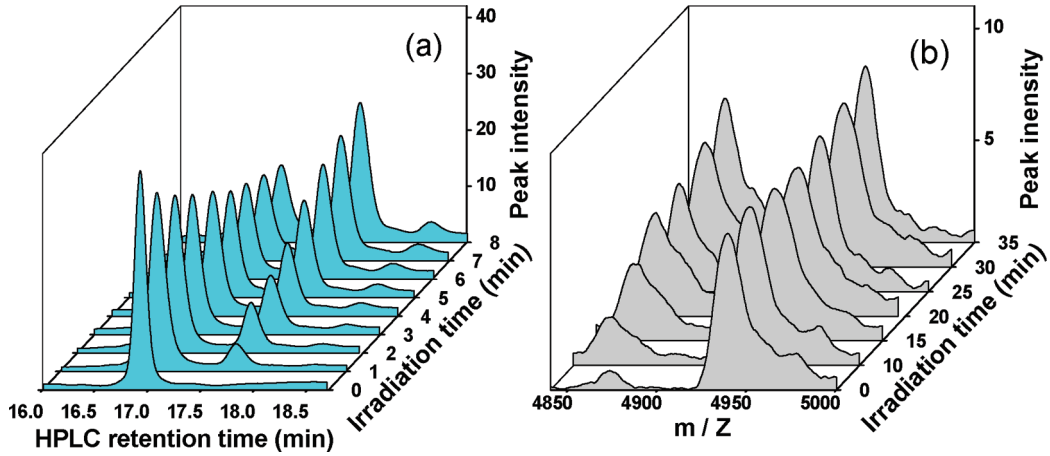

Figure 4. (a) Conversion of **PyA-2^{Br}U** to **PyA-2U** monitored by HPLC and (b) conversion of **PyA-4^{Br}U** to **PyA-4U** monitored by MALDI mass spectrometry.

the **PyA$^{+\bullet}$-PI$^{-\bullet}$** charge-separated state. The 450 nm band has a band maximum similar to that reported for a urea-linked pyrene-nitrobenzene dyad,[23] and the 420 nm shoulder is similar to the maximum of the long-wavelength band of electrochemically generated PI$^{-\bullet}$.[24] Analysis of the transient spectra provides a charge-separation time of 480 ps for the **PyA-PI** (Table 1). Charge recombination is slow on the 1.9 ns time scale of our measurements.

Pump−Probe Spectra for the PyA Conjugates. The transient spectra for **PyA-AT**, **-1^{Br}U**, and **-2^{Br}U** are shown in Figure 3. As is the case for **PyA-H**, formation and decay of the pyrene ^{2}S* 575 nm band for all of the PyA conjugates occur during the initial 1 ps following the laser pump pulse and is accompanied by the growth of the ^{1}S* absorption bands at 375 and 525 nm. The 525 nm bands in the transient absorption spectra of **PyA-AT** (Figure 3a) and the other PyA conjugates are broader and more symmetric than the corresponding band of **PyA-H** (Figure 2a). Global fitting of the transient absorption bands of **PyA-AT** and **PyA-*n*-^{Br}U** (n = 1−4) provides rising components having a time constant of 5−10 ps (assigned to relaxation of ^{1}S*) and either one or two decay components (Table 1). The longer lived decay components (>2 ns) observed in both the global fits and 375 and 525 nm single wavelength decays are assigned to ^{1}S* (see Discussion Section).

The transient spectra of **PyA-1^{Br}U** and **-2^{Br}U** (Figure 3b,c), but not the other **PyA** conjugates, display formation of 470 nm bands that are assigned to **PyA$^{+\bullet}$** on the basis of comparison with the transient spectra of **PyA-PI** (Figure 2b). The ratio of the 525/345 nm band intensities is also smaller for these conjugates (and for **PyA-PI**) than for the other **PyA** conjugates. The rise times for the 470 nm bands of **PyA-1^{Br}U** and **-2^{Br}U** determined from the ratio of the 470/520 nm intensities of the band maxima are 44 and 18 ps, respectively (Table 1). The rise time for **PyA-1^{Br}U** is similar to the 30 ps rising component obtained from global fitting and somewhat faster than the 140 ps fluorescence decay time. Decay times of ca. 150 and 300 ps assigned to charge recombination are obtained from the 470/425 nm band intensity ratios and global fitting of the transient absorption bands of **PyA-1^{Br}U** and **-2^{Br}U**, respectively (Table 1). A 470 nm shoulder is not observed in the transient spectra of **PyA-AT**, **-3^{Br}U**, or **-4^{Br}U** (spectra not shown).

Photochemistry of the PyA Conjugates. Dilute solutions of the PyA conjugates containing 0.1 M NaCl and 0.1 M *i*-PrOH were irradiated on an optical bench with monochromatic 355 nm light corresponding to the pyrene absorption maxima. The use of *i*-PrOH as an efficient scavenger for the uracilyl radical formed upon loss of bromide from ^{Br}U has been described by Sugiyama and Saito[25] and employed in our recent study of APy conjugates.[12] Aliquots were removed and analyzed periodically either directly by HPLC with UV diode array detection or by MALDI-TOF mass spectrometry analysis of samples collected by HPLC.

Conjugate **PyA-AT** is stable under our 355 nm irradiation conditions, as are the control sequences **3^{Br}U** and **4^{Br}U** (Figure S4, Supporting Information). Product peaks corresponding to loss of bromide and formation of uracil-containing conjugates were observed for all of the ^{Br}U-containing PyA conjugates. Loss of bromide was confirmed by mass spectrometry of the major product peaks collected by HPLC. In the case of **PyA-1^{Br}U**, two product peaks of similar size were observed. For this reason, this conjugate was not included in our quantitative photochemical studies. The reactant and product peaks of conjugates **PyA-2−4^{Br}U** can be resolved by HPLC under nondenaturing conditions, as shown in Figure 4a for the conversion of **PyA-2^{Br}U** to **PyA-2U** with increasing irradiation time. Integrated peak areas display good mass balance (ca. 90% at 50% conversion). Reactant and product peak separation decreases as the distance between the pyrene capping group

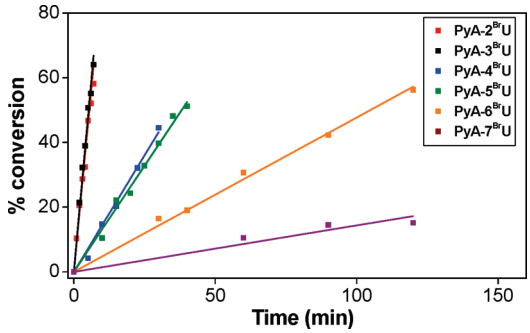

Figure 5. Time evolution for the formation of **PyA-*n*U** conjugates upon 355 nm irradiation of **PyA-*n*^{Br}U** conjugates in aqueous buffer containing 0.1 M *i*-PrOH.

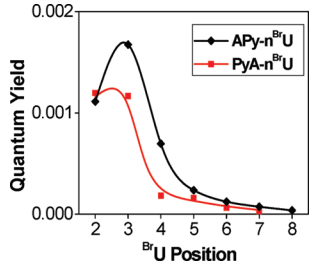

Figure 6. Quantum yields for loss of bromide from **APy-*n*^{Br}U** and **PyA-*n*^{Br}U** conjugates in aqueous buffer containing 0.1 M *i*-PrOH.

and ^{Br}U increases, necessitating the use of MALDI analysis for the **PyA-5−7^{Br}U** conjugates. In the case of **PyA-4^{Br}U**, analysis by both HPLC and MALDI (Figure 4b) provides essentially identical data for conversion vs irradiation time (Figure S5, Supporting Information).

Plots of conversion vs irradiation time for the conjugates **PyA-2−7^{Br}U** obtained from HPLC and MALDI data are shown in Figure 5. The initial slopes of these plots provide relative quantum yields for the formation of **PyA-*n*U**. Absolute quantum yields (Φ_U) for **PyA-4^{Br}U** were determined using monochromatic irradiation of the pyrene chromophore and potassium ferrioxalate chemical actinometry.[18] The resulting values of Φ_U for the PyA conjugates are shown in Figure 6 along with our previously published results for APy conjugates.[12] The absolute values of Φ_U are small; however, our analytical methods permit accurate determination of Φ_U.

The photochemical behavior of the conjugates **PyA-2,3^{Br}U** and **PyA-2,4^{Br}U** (Chart 1c) which possess two ^{Br}U bases has also been investigated. HPLC traces for irradiation of these conjugates are provided in Figure S6 and S7, Supporting Information, and plots of conversion vs time are shown in Figure 7. In the case of **PyA-2,3^{Br}U**, the two monobromides **PyA-2U,3^{Br}U** and **PyA-2^{Br}U,3U** are both primary photoproducts formed in an initial ratio of ca. 2:1 (Figure 7a). Upon further irradiation, both products are converted to **PyA-2,3U**. In the case of **PyA-2,4^{Br}U**, the monobromide **PyA-2U,4^{Br}U** is the only primary photoproduct. It is converted to **PyA-2,4U** upon further irradiation (Figure 7b).

Discussion

Conjugate Structure and Energetics of Hole and Electron Injection. Pyrene derivatives have been widely employed in studies of DNA electron transfer.[12,13,26,27] The singlet states of pyrene derivatives can serve as an electron acceptor and/or donor, depending upon the pyrene substituent and the choice of nucleobase quencher. For example, we find that the pyrenecarboxamide PyA can serve as an electron acceptor capable of the reduction of G, but not A,[14] and as an electron donor capable of the oxidation of ^{Br}U but not T (Figure 1b).

Pyrene and other aromatic chromophores tethered to the 5′- or 3′-terminus of a duplex or hairpin usually are assumed to adopt an end-capping geometry in which one face of the chromophore is π-stacked with the terminal base pair and the other face is exposed to water (Figure 8a).[27,28] An end-capped geometry has been established by solution NMR studies for a 5′-tethered stilbene derivative;[29] however, alternative geometries have been observed for larger, more hydrophobic aromatics.[30] We recently reported that a PyA conjugate possessing a single G−C base pair adopts an intercalated hairpin conformation in which PyA is π-stacked with a G−C at the second base pair in preference to an end-capped conformation in which it is π-stacked with the terminal base pair (Figure 8b).[14] The intercalated structure nicely explains the observation of efficient hole injection to G−C base pairs located in either of the two terminal base pairs but not elsewhere in the hairpin structure. The observation of dual exponential fluorescence decay for **PyA-AT** and the **PyA-*n*^{Br}U** conjugates (Table 1) is also consistent with the presence of two kinetically nonequivalent conformations.

The energetics of hole and electron injection from **PyA** to a neighboring electron acceptor or donor can be estimated using Weller's equation (eq 1)

$$\Delta G_{et} = -E_s - (E_{rdn} - E_{ox}) + (2.6/\varepsilon - 0.13\ \text{eV}) \quad (1)$$

where E_s is the singlet energy of **PyA-H**; E_{ox} and E_{rdn} are oxidation and reduction potentials of PyA and the nucleobases (Chart 1a,b); and the final term is an empirical correction for the solvent-dependent Coulomb attraction energy (−0.06 eV in acetonitrile).[31] The redox potentials of both PyA and the bases are not expected to be precisely the same for the hairpin structures in aqueous solution as for the isolated molecules in polar aprotic solvents. Thus, the free energies for formation of the charge-separated states obtained using eq 1 and shown in Figure 1 are approximate values. However, the estimated energies of the contact radical ion pairs (Figure 1b) are consistent with the observation of fluorescence quenching of PyA by G but not A[14] and by ^{Br}U but not T (Table 1). Similarly, the value of $\Delta G_{et} = -0.5$ eV for the dyad **PyA-PI** calculated from the phthalimide reduction potential (−1.40 V) is consistent with the observation of efficient PyA fluorescence quenching by PI (Table 1).

Dynamics of Electron Injection and Charge Recombination. The transient absorption spectra for all of the **PyA** conjugates display rapid decay (<1 ps) of the ^{2}S* 575 nm band and formation of ^{1}S* 375 and 525 nm bands. The ^{1}S* band intensities continue to increase with rise times of 6−10 ps attributed to ^{1}S* relaxation, independent of the location of ^{Br}U (Table 1). In addition to these bands, the transient absorption spectra of **PyA-1^{Br}U** and **-2^{Br}U** (Figure 3b,c) but not the other PyA conjugates display bands at 470 nm which are assigned to the formation of the **PyA$^{+\bullet}$-^{Br}U$^{-\bullet}$** contact radical ion pair, on the basis of their similarity to the 450 nm band in the transient absorption spectrum of the dyad **PyA-PI** (Figure 1b). The rise times for the 470 nm bands determined from the 470/520 nm band intensity ratios are 44 ps for **PyA-1^{Br}U** and 18 ps for **PyA-2^{Br}U** (Table 1). These rise times for electron injection are similar to the hole injection times for **PyA-1G** and **-2G**, in accord with the similar energetics for electron injection to ^{Br}U and hole injection to G (Figure 1b). Faster hole and electron injection for **PyA-2G** vs **-1G** and **PyA-2^{Br}U** vs **-1^{Br}U** plausibly reflects

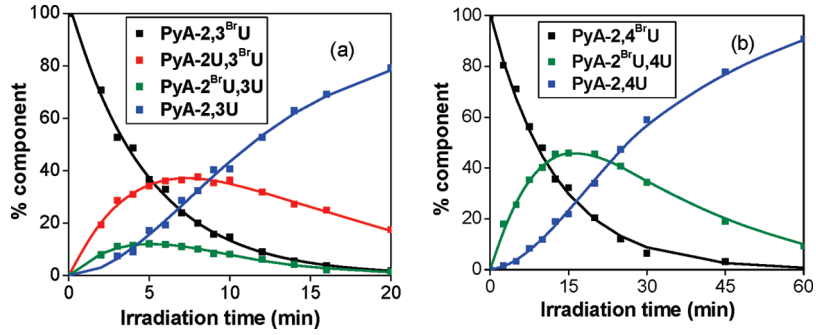

Figure 7. Time-dependent composition of reduction products formed during 355 nm irradiation of (a) **PyA-2,3^{Br}U** and (b) **PyA-2,4^{Br}U** in standard buffer with 0.1 M isopropanol.

Figure 8. Cartoon from ref 14 showing a duplex having a 5′- or 3′-tethered chromophore (yellow oblong box) serving as a capping group (a) or intercalated between the first and second base pairs (b).

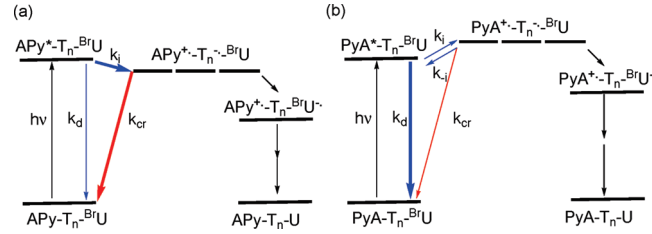

Figure 9. Kinetic scheme for photoinduced charge separation in (a) APy and (b) PyA conjugates. Bold arrows indicate major decay pathways.

better π-stacking of PyA with the second base pair in an intercalated structure (Figure 8b). The long-lived components of **PyA-1^{Br}U** and **-2^{Br}U** transient decay and fluorescence decay are attributed to conformations in which PyA is not well-stacked with the BrU−A base pair.

The observation of efficient charge separation by transient absorption spectroscopy only when PyA and ^{Br}U (or G[14]) are nearest neighbors is reminiscent of the photooxidation of G−C base pairs by an intercalated acridium dye[32] or by a perylene-dicarboxamide hairpin linker,[33] both of which are relatively weak electron acceptors. All of these systems display strong distance dependence with little or no electron transfer when ^{Br}U or G is separated from the chromophore by even one A−T base pair. Such strong distance dependence is indicative of a very large value of β, the distance dependence for single-step superexchange electron transfer, in these systems. Strong distance dependence has also been observed for the ethidium−nitroindole donor−acceptor system studied by Fiebig and Wagenknecht.[34] This system displays a minor component of moderately rapid transient decay (50 ps, 22% amplitude) and a major component of long-lived decay (>2 ns), attributed to poorly stacked conformations, when a single A:T base pair separates the donor and acceptor.

The **PyA** conjugates all have long-lived transient decay components (>2 ps) assigned to ^{1}S* radiative and nonradiative decay, in accord with the observation of long fluorescence decay times (Table 1). **PyA-1^{Br}U** and **PyA-2^{Br}U** also have shorter-lived transient decay components assigned to charge recombination of the **PyA$^{+\bullet}$-^{Br}U$^{-\bullet}$** contact radical ion pairs. The decay times of 130 and 240 ps obtained from global fitting are similar to those obtained from the 470/520 nm band intensity ratios (Table 1). These decay times are substantially longer than those for the corresponding APy conjugates which have decay times of 2.4 and 4.4 ps, respectively.[12] Thus the higher energy of the **PyA$^{+\bullet}$-^{Br}U$^{-\bullet}$** vs **APy$^{+\bullet}$-^{Br}U$^{-\bullet}$** radical ion pairs results in slower recombination for the PyA conjugates, as expected for an electron transfer process in the Marcus inverted region.[35] The somewhat longer charge recombination vs charge separation times for **PyA-1^{Br}U** and **PyA-2^{Br}U** permit observation of their radical ion pair transient absorption spectra, which was not possible in the case of the **PyA$^{-\bullet}$-G$^{+\bullet}$** contact radical ion pair as a consequence of inverted kinetics.[14]

Photochemical Behavior of the PyA-*n*^{Br}U Conjugates. The protocol developed for determining the quantum yields for conversion of the **APy-*n*^{Br}U** conjugates to **APy-*n*U** has been employed in our studies of the **PyA-*n*^{Br}U** conjugates.[12] To briefly summarize, photoinduced charge separation followed by loss of bromide from ^{Br}U$^{-\bullet}$ results in formation of the uracilyl radical, which is scavenged efficiently by 0.1 M *i*-PrOH with formation of the **PyA-*n*U** conjugate. In the absence of either ^{Br}U (**PyA-AT**) or PyA (**3^{Br}U** and **4^{Br}U**, Chart 1c), no products are formed upon irradiation. Direct irradiation of ^{Br}U-containing duplexes at 308 nm results in loss of bromide;[25] however, ^{Br}U does not absorb the 355 nm irradiation used in our studies.

The initial slopes of plots of conversion of **PyA-*n*^{Br}U** conjugates to **PyA-*n*U** conjugates vs irradiation time (Figure 5) provide relative quantum yields, which can be converted to absolute quantum yields (Φ_U) by comparison with the quantum yield for **PyA-4^{Br}U** determined using ferrioxalate actinometry. A plot of Φ_U vs the position of ^{Br}U in the hairpin conjugate is remarkably similar to that previously reported for the **APy-*n*^{Br}U** conjugates (Figure 6). The low values of Φ_U for the **APy-*n*^{Br}U** conjugates were attributed to efficient charge separation followed by fast charge recombination in the **APy$^{+\bullet}$-T$^{-\bullet}$** contact ion pairs (Figure 9a).[12] The absence of fluorescence quenching or formation of the PyA$^{+\bullet}$ in the transient absorption spectrum of **PyA-3^{Br}U** and **-4^{Br}U** suggests that formation of **PyA$^{+\bullet}$-T$^{-\bullet}$** contact ion pairs is inefficient (Figure 9b), presumably due to slow, reversible endergonic electron injection to neighboring T−A base pairs. Thus, the dominant energy-wasting processes for the PyA conjugates are radiative and nonradiative decay of singlet PyA. As is the case for APy conjugates, loss of bromide in the PyA systems presumably occurs via inefficient electron transport that competes with reversible electron injection (k_{-i}).

A plot of ln(Φ_U) vs the distance between PyA and ^{Br}U for **PyA-*n*^{Br}U** ($n > 2$) calculated assuming an end-capping conformation and a π-stacking distance of 3.4 Å has a slope of $\beta =$

0.26 ± 0.4 Å^{-1} (Figure S8, Supporting Information), similar to the value for the **APy-*n*^{Br}U** conjugates ($\beta = 0.22 \pm 2$ Å^{-1}).[12] Both values are somewhat larger than those reported for several other electron transport systems including flavin-sensitized cleavage of the $T<>T$ dimer ($\beta = 0.11$ Å^{-1}),[4] flavin-sensitized cleavage of thymine oxetane ($\beta = 0.16$ Å^{-1}),[7] and Ir(III)-sensitized loss of bromide from ^{Br}U ($\beta = 0.12$ Å^{-1}).[10] However, the linear nature of these plots and their similar slopes is suggestive of a common mechanism for electron transport in duplex DNA. We previously noted that the distance dependence for Φ_U in the APy system is similar to that for the quantum yield for A-tract hole transport in capped hairpins having a stilbenedicarboxamide capping group and a stilbenediether linker which serve as electron acceptor and donor, respectively ($\beta = 0.16$ Å^{-1}).[12] The similar distance dependence for DNA hole and electron transport may reflect a similar rate-determining process such as conformational gating for both processes.

Photochemical Behavior of the PyA-2,3^{Br}U and PyA-2,4^{Br}U Conjugates. The dibromides **PyA-2,3^{Br}U** and **PyA-2,4^{Br}U** undergo loss of both bromides upon prolonged irradiation resulting in the formation of **PyA-2,3U** and **PyA-2,4U**, respectively (Figures S6 and S7, Supporting Information, and Figure 7). Induction periods are observed for the formation of **PyA-2,3U** and **PyA-2,4U**, indicating that that a single photon effects the formation of a single uridine, as expected for a mechanism in which loss of bromide removes the excess negative charge leaving an uncharged conjugate. Giese et al. observed that a single photoinjected electron can repair more than one thymine dimer as the negative charge is retained after dimer cleavage.[5] The loss of the second bromide from **PyA-2,4^{Br}U** is slower than that from **PyA-2,3^{Br}U** (Figure 7b), in accord with a consecutive reaction process, and with the lower quantum yield for the monobromide **PyA-4^{Br}U** vs **PyA-3^{Br}U**.

In the case of **PyA-2,3^{Br}U**, the primary products **PyA-2U,3^{Br}U** and **PyA-2^{Br}U,3U** are formed with an initial ratio of ca. 2:1 (Figure 7a). The preference for loss of the 5′-bromide is analogous to the preference for oxidative cleavage at the 5′-G in a GG step.[36] This result is consistent with either a localized anion radical with relatively rapid electron migration from reduced 2^{Br}U to 3^{Br}U or a delocalized anion radical with faster loss of bromide from 2^{Br}U vs 3^{Br}U. The distinction between localized and delocalized $^{Br}U^{Br}U$ steps remains to be explored, while the debate among theoreticians over the extent of hole delocalization in GG steps continues.[37]

In the case of **PyA-2,4^{Br}U**, the major primary product is **PyA-2U,4^{Br}U** (Figure 7b). This indicates that electron transport in the 5′-2^{Br}UT4^{Br}U triad is unable to compete with loss of bromide from reduced $2^{Br}U^{-\bullet}$, as previously observed by Ito and co-workers for the 2^{Br}UC 4^{Br}U triad using a covalently linked phenothiazine to effect photochemical electron injection.[9] Rivera and Schuler report a rate constant of 1.4×10^8 s^{-1} for loss of bromide from reduced ^{Br}U.[38] Assuming a similar rate constant for loss of bromide in the base paired hairpin, the rate constant for 2^{Br}U T 4^{Br}U electron transport can be no faster than 10^7 s^{-1} and still be consistent with our experimental results (Figure 7b). We previously reported that hole transport in the a GAG triad occurs with a rate constant of ca. 10^7 s^{-1}.[39] Thus, the rate constant for single-step electron transport in a triad system is comparable to or slower than that for hole transport. Furthermore, since loss of bromide terminates the electron transport process, ^{Br}U cannot be used to study multiple-step hopping processes analogous to those observed for hole hopping between G hole traps.

Concluding Remarks. The singlet state of PyA can serve as a weak electron donor, capable of selective electron injection to ^{Br}U vs the natural pyrimidines, as well as a weak electron acceptor, capable of hole injection to G, but not A (Figure 1b).[14] Electron and hole injection are observed only when the bases ^{Br}U or G, respectively, are nearest neighbors to PyA. The absence of spectroscopic evidence for electron transfer over even a single intervening A−T base pair indicates that single-step superexchange (tunneling) is inefficient in these systems even at relatively modest donor−acceptor distances (6.8 Å). This in turn suggests that superexchange is strongly distance dependent ($\beta > 1$ Å^{-1}), as previously observed for other systems in which electron or hole injection into the bridging base pairs is highly endergonic.[15,32−34] These observations are consistent with the proposal of Beratan et al. that the tunneling energy gap determines β, a large gap resulting in a large value of β.[40] The higher energies of charge separated vs contact radical ion pairs may also account for the large values of β in these systems.

Photoreduction of ^{Br}U in the conjugates **PyA-*n*^{Br}U** when $n \geq 3$ most likely occurs via endergonic charge separation followed by electron transport from the **PyA$^{+\bullet}$-T$^{-\bullet}$** contact radical ion pair to ^{Br}U (Figure 9b). Reversible electron injection followed by slow electron transport can account for the absence of fluorescence quenching for **PyA-*n*^{Br}U** when $n \geq 3$ (Table 1) as well as the low quantum yields for product formation from these conjugates (Figure 6). When ^{Br}U is adjacent to PyA, the **PyA$^{+\bullet}$-^{Br}U$^{-\bullet}$** contact radical ion pair presumably is formed irreversibly. However, charge recombination is more rapid than loss of bromide, resulting in a low quantum yield for product formation from **PyA-2^{Br}U** (Figure 6). The quantum yields for loss of bromide from the PyA conjugates decrease by a factor of 2 for each additional A−T base pair separating PyA and ^{Br}U, a distance dependence similar to that observed for other DNA electron and hole transport systems.[4,7,10,14] This suggests that both hole and electron transport occur by relatively slow multistep hopping mechanisms, the dynamics of which may be subject to conformational control.

Acknowledgment. This research is supported by grants from the Chemical Sciences, Geosciences and Biosciences Division, Office of Basic Energy Sciences, Office of Science, U.S. Department of Energy (DE-FG02-96ER14604 to FDL), the National Science Foundation (CHE-0628130 to TF).

Supporting Information Available: MALDI-TOF analysis for capped hairpins, circular dichroism spectra, thermal dissociation profiles, ZINDO-derived UV spectra, plots of conversion vs irradiation time obtained from HPLC and MALDI analysis of **PyA-4^{Br}U**, HPLC traces for irradiated solutions of conjugates containing two bromouracils, and a plot of the distance dependence of the quantum yield for product formation. This material is available free of charge via the Internet at http://pubs.acs.org.

References and Notes

(1) (a) Lewis, F. D. *Electron Transfer in Chemistry*; Balzani, V., Ed.; Wiley-VCH: Weinheim, Germany, 2001; Vol. 3, pp 105−175. (b) Schuster, G. B., Ed. *Long-Range Charge Transfer in DNA, I and II*; Springer, 2004; Vol. 236, *237*. (c) Wagenknecht, H. A. *Charge Transfer in DNA*; Wiley-VCH: Weinheim, 2005.

(2) Seidel, C. A. M.; Schulz, A.; Sauer, M. H. M. *J. Phys. Chem.* **1996**, *100*, 5541–5553.

(3) (a) Schwögler, A.; Burgdorf, L. T.; Carell, T. *Angew. Chem., Int. Ed.* **2000**, *39*, 3918–3920. (b) Breeger, S.; Hennecke, U.; Carell, T. *J. Am. Chem. Soc.* **2004**, *126*, 1302–1303.

(4) Behrens, C.; Burgdorf, L. T.; Schwogler, A.; Carell, T. *Angew. Chem., Int. Ed.* **2002**, *41*, 1763–1766.

(5) Giese, B.; Carl, B.; Carl, T.; Carell, T.; Behrens, C.; Hennecke, U.; Schiemann, O.; Feresin, E. *Angew. Chem., Int. Ed.* **2004**, *43*, 1848–1851.

(6) Carell, T.; Behrens, C.; Gierlich, J. *Org. Biomol. Chem.* **2003**, *1*, 2221–2228.

(7) Stafforst, T.; Diederichsen, U. *Angew. Chem., Int. Ed.* **2006**, *45*, 5376–5380.

(8) (a) Ito, T.; Rokita, S. E. *J. Am. Chem. Soc.* **2003**, *125*, 11480–11481. (b) Ito, T.; Rokita, S. E. *J. Am. Chem. Soc.* **2004**, *126*, 15552–15559. (c) Manetto, A.; Breeger, S.; Chatgilialoglu, C.; Carell, T. *Angew. Chem., Int. Ed.* **2006**, *45*, 318–321.

(9) Ito, T.; Kondo, A.; Terada, S.; Nishimoto, S. *J. Am. Chem. Soc.* **2006**, *128*, 10934–10942.

(10) Elias, B.; Shao, F. W.; Barton, J. K. *J. Am. Chem. Soc.* **2008**, *130*, 1152–1153.

(11) Kawai, K.; Kimura, T.; Kawabata, K.; Tojo, S.; Majima, T. *J. Phys. Chem. B* **2003**, *107*, 12838–12841.

(12) Daublain, P.; Thazhathveetil, A. K.; Wang, Q.; Trifonov, A.; Fiebig, T.; Lewis, F. D. *J. Am. Chem. Soc.* **2009**, *131*, 16790–16797.

(13) (a) Kaden, P.; Mayer-Enthart, E.; Trifonov, A.; Fiebig, T.; Wagenknecht, H.-A. *Angew. Chem., Int. Ed.* **2005**, *44*, 1636–1639. (b) Gaballah, S. T.; Collier, G.; Netzel, T. L. *J. Phys. Chem. B* **2005**, *109*, 12175–12181.

(14) Siegmund, K.; Daublain, P.; Wang, Q.; Trifonov, A.; Fiebig, T.; Lewis, F. D. *J. Phys. Chem. B* **2009**, *113*, 16276–16284.

(15) Lewis, F. D.; Zhu, H.; Daublain, P.; Fiebig, T.; Raytchev, M.; Wang, Q.; Shafirovich, V. *J. Am. Chem. Soc.* **2006**, *128*, 791–800.

(16) Berlman, I. B. *Handbook of Fluorescence Spectra of Aromatic Molecules*, 2nd ed.; Academic Press: New York, 1971.

(17) Astruc, D. *Electron Transfer in Chemistry*; Balzani, V., Ed.; Wiley-VCH: Weinheim, 2001; Vol. 2.

(18) Murov, S. L. *Handbook of Photochemistry*; Marcel Dekker: New York, 1973.

(19) Alfred, J.-C.; Daunis, J.; Jacquier, R. *Macromol. Chem. Phys.* **1996**, *197*, 389–401.

(20) Johnson, W. C. *Circular Dichroism, Principles and Applications*; Berova, N., Nakanishi, K., Woody, R. W., Eds.; Wiley-VCH: New York, 2000; pp 741−768.

(21) CAChe *CAChe Release 6.1.10*, 2000.

(22) Raytchev, M.; Pandurski, E.; Buchvarov, I.; Modrakowski, C.; Fiebig, T. *J. Phys. Chem. A* **2003**, *107*, 4592–4600.

(23) Lewis, F. D.; Daublain, P.; Delos Santos, G.; Liu, W.; Asatryan, A. M.; Markarian, S. A.; Fiebig, T.; Raytchev, M.; Wang, Q. *J. Am. Chem. Soc.* **2006**, *128*, 791–800.

(24) Gosztola, D.; Niemczyk, M. P.; Svec, W.; Lukas, A. S.; Wasielewski, M. R. *J. Phys. Chem. A* **2000**, *104*, 6545–6551.

(25) (a) Sugiyama, H.; Tsutsumi, Y.; Saito, I. *J. Am. Chem. Soc.* **1990**, *112*, 6720–6721. (b) Fujimoto, K.; Sugiyama, H.; Saito, I. *Tetrahedron Lett.* **1998**, *39*, 2137–2140.

(26) (a) Shafirovich, V. Y.; Dourandin, A.; Luneva, N. P.; Geacintov, N. E. *J. Phys. Chem. B* **1997**, *101*, 5863–5868. (b) Geacintov, N. E.; Solntsev, K.; Johnson, L. W.; Chen, J. X.; Kolbanovskiy, A. D.; Liu, T. M.; Shafirovich, V. Y. *J. Phys. Org. Chem.* **1998**, *11*, 561–565.

(27) Zahavy, E.; Fox, M. A. *J. Phys. Chem. B* **1999**, *103*, 9321–9327.

(28) (a) Mann, J. S.; Shibata, Y.; Meehan, T. *Bioconjugate Chem.* **1992**, *3*, 554–558. (b) Schuster, G. B. *Acc. Chem. Res.* **2000**, *33*, 253–260. (c) Lewis, F. D.; Zhang, L.; Liu, X.; Zuo, X.; Tiede, D. M.; Long, H.; Schatz, G. S. *J. Am. Chem. Soc.* **2005**, *127*, 14445–14453.

(29) Tuma, J.; Connors, W. H.; Stitelman, D. H.; Richert, C. *J. Am. Chem. Soc.* **2002**, *124*, 4236–4246.

(30) (a) Siegmund, K.; Maheshwary, S.; Narayanan, S.; Connors, W.; Riedrich, M.; Printz, M.; Richert, C. *Nucleic Acids Res.* **2005**, *33*, 4838–4848. (b) Tuma, J.; Paulini, R.; Stütz, J. A. R.; Richert, C. *Biochemistry* **2004**, *43*, 15680–15687.

(31) Weller, A. *Zeit. Phys. Chem. Neue. Folg.* **1982**, *133*, 93–98.

(32) (a) Hess, S.; Götz, M.; Davis, W. B.; Michel-Beyerle, M. E. *J. Am. Chem. Soc.* **2001**, *123*, 10046–10055. (b) von Feilitzsch, T.; Tuma, J.; Neubauer, H.; Verdier, L.; Haselsberger, R.; Feick, R.; Gurzadyan, G.; Voityuk, A. A.; Griesinger, C.; Michel-Beyerle, M. E. *J. Phys. Chem. B* **2008**, *112*, 973–989.

(33) Lewis, F. D.; Zhang, L.; Kelley, R. F.; McCamant, D.; Wasielewski, M. R. *Tetrahedron* **2007**, *63*, 3457–3464.

(34) Valis, L.; Wang, Q.; Raytchev, M.; Buchvarov, I.; Wagenknecht, H. A.; Fiebig, T. *Proc. Natl. Acad. Sci. U.S.A.* **2006**, *103*, 10192–10195.

(35) Marcus, R. A. *J. Chem. Phys.* **1965**, *43*, 679–701.

(36) (a) Saito, I.; Takayama, M.; Sugiyama, H.; Nakatani, K. *J. Am. Chem. Soc.* **1995**, *117*, 6406–6407. (b) Sugiyama, H.; Saito, I. *J. Am. Chem. Soc.* **1996**, *118*, 7063–7068.

(37) (a) Conwell, E. M.; Basko, D. M. *J. Am. Chem. Soc.* **2001**, *123*, 11441–11445. (b) Kurnikov, I. V.; Tong, G. S. M.; Madrid, M.; Beratan, D. N. *J. Phys. Chem. B* **2002**, *106*, 7–10.

(38) Rivera, E.; Schuler, R. H. *J. Phys. Chem.* **1983**, *87*, 3966–3971.

(39) Lewis, F. D.; Liu, J.; Zuo, X.; Hayes, R. T.; Wasielewski, M. R. *J. Am. Chem. Soc.* **2003**, *125*, 4850–4861.

(40) Lewis, F. D.; Liu, J.; Weigel, W.; Rettig, W.; Kurnikov, I. V.; Beratan, D. N. *Proc. Natl. Acad. Sci. U.S.A.* **2002**, *99*, 12536–12541.

JP9107393